Title:

Environmental calibration of coral luminescence as a proxy for terrigenous dissolved organic carbon concentration in tropical coastal oceans

Author names and affiliations

Nikita Kaushal, Asian School of the Environment, Nanyang Technological University, Singapore

Now at Department of Earth Sciences, ETH Zurich, Switzerland

nkaushal@ethz.ch / nikitageologist@gmail.com

Orcid: 0000-0002-2220-9046

Jani T. I. Tanzil, St. John's National Marine Laboratory, National University of Singapore, Singapore

Tropical Marine Science Institute, National University of Singapore, Singapore

jani.tanzil@nus.edu.sg

Orcid: 0000-0002-8072-5014

Yongli Zhou, Asian School of the Environment, Nanyang Technological University, Singapore

yzhou@mbl.edu

Now at Marine Biological Laboratory, Woods Hole, MA 02543, United States of America

Orcid: 0000-0001-8403-6315

Maria Rosabelle Ong, Department of Earth and Environmental Sciences, Lamont-Doherty Earth Observatory, Columbia University, United States of America
Department of Earth and Planetary Sciences, American Museum of Natural History, United States of America
mong@amnh.org
Orcid: 0000-0001-9271-4083

Nathalie F. Goodkin, Asian School of the Environment, Nanyang Technological University, Singapore
Earth Observatory of Singapore, Nanyang Technological University, Singapore
Department of Earth and Planetary Sciences, American Museum of Natural History, United States of America
ngoodkin@amnh.org
Orcid: 0000-0001-9697-5520

Patrick Martin, Asian School of the Environment, Nanyang Technological University, Singapore
pmartin@ntu.edu.sg
Orcid: 0000-0001-8008-5558

Highlights

- Coral luminescence green-to-blue ratio (coral G/B) is a quantitative proxy for terrigenous dissolved organic carbon concentration in river-influenced tropical coastal oceans.

- Coral G/B can also be used to reconstruct the absorption spectrum of terrigenous chromophoric dissolved organic matter (CDOM) over the wavelength range 230-550 nm.
- Downcore luminescence G/B variability can therefore be used to investigate temporal variability in tDOC input and its impacts on optical water quality.

Abstract

The riverine flux of terrigenous dissolved organic matter (tDOM) to the ocean is a significant contributor to the global carbon cycle. In response to anthropogenic drivers such as land-use change the flux is expected to increase, and this may impact both the availability of sunlight in coastal ecosystems, and the seawater carbonate system and coastal CO_2 fluxes. Yet despite its biogeochemical and ecological significance, there are few long-term and high-resolution time series of tDOM parameters. Corals incorporate fluorescent tDOM molecules from the chromophoric dissolved organic matter (CDOM) pool in their skeletons, and the resulting luminescence variability in coral skeleton cores has traditionally been used to reconstruct hydroclimate variation. Here, we use two replicate coral cores and concurrent in-situ biogeochemical data from the Sunda Sea Shelf in Southeast Asia, where coastal peatlands supply high tDOM inputs, to show that variability in coral luminescence green-to-blue ratios (coral G/B) can be used to quantitatively reconstruct the concentration of terrigenous dissolved organic carbon (tDOC). Moreover, coral G/B can be used to reconstruct the full absorption spectrum of CDOM from 230–550 nm, as well as the specific ultraviolet absorbance at 254 nm ($SUVA_{254}$) of the DOM pool. Comparison to a core from Borneo shows that there may be site-specific offsets in the G/B–CDOM absorption relationship, but that the slope of the relationship is very similar, validating the robustness of the proxy. By demonstrating that coral cores can be used to estimate past changes in coastal tDOC and CDOM, we establish a method to study

natural and anthropogenic drivers of land–ocean tDOM fluxes and their ecological consequences in tropical coastal seas over decadal to centennial time scales.

Keywords

corals, luminescence G/B, tDOC, CDOM, dissolved organic matter, Southeast Asia, peatlands

1. Introduction

The transfer of terrigenous Dissolved Organic Carbon (tDOC) from land to the coastal ocean is a significant flux in the global carbon cycle (Le Quéré et al., 2013). Tropical rivers contribute nearly two-thirds of the global land-to-ocean tDOC flux (Dai et al., 2012). Moreover, this flux appears to have been considerably perturbed by human activity in recent times (Butman et al., 2015; Monteith et al., 2007; Noacco et al., 2017). Long-term increases in surface water DOC across North America and Europe are largely attributed to the recovery of ecosystems from historical atmospheric pollution (Monteith et al., 2007), although anthropogenic landscape alterations (Butman et al., 2015; Noacco et al., 2017) and climatic changes and permafrost thaw (de Wit et al., 2016; Larsen et al., 2011; Wauthy et al., 2018) are also implicated. In tropical regions, deforestation destabilizes soil organic carbon pools (Evans et al., 2014) and can lead to either net increases (Moore et al., 2013; Sanwlani et al., 2022) or net decreases (Drake et al., 2019) in riverine tDOC flux, depending on the lability of the newly mobilized soil carbon.

The environmental consequences of changing tDOC fluxes to the ocean depend on the biogeochemical fate of tDOC at sea, which remains poorly understood (Ciais et al., 2014). In parts of the Arctic and Southeast Asia, extensive remineralization of tDOC results in coastal seawater acidification and eventually degassing of CO_2 to the atmosphere (Wit et al., 2018; Zhou et al., 2021). tDOC is also rich in chromophoric dissolved organic matter (CDOM), which is that fraction of DOM that absorbs light. Increased fluxes of terrigenous CDOM can thus reduce underwater light availability and spectral quality in coastal waters (Urtizberea et al., 2013).

Despite the significance of tDOC and CDOM, long time series of their fluxes and concentrations in coastal waters are only available in parts of Europe and North America. Although CDOM and DOC can be estimated by satellite remote sensing (Sanwlani et al., 2022) accurate remote sensing in optically complex coastal waters requires extensive optical and biogeochemical field data for algorithm development, which limits the widespread use of this technique. Moreover, satellite remote sensing can only provide data over the most recent few decades. Longer records are required to understand the impact of anthropogenic changes that pre-date the satellite era, as well as long-term and cyclical drivers of terrigenous CDOM and tDOC variability such as temperature and hydrology. It is therefore necessary to find a paleoproxy to reconstruct terrigenous dissolved organic matter (tDOM) parameters.

In the absence of measured instrumental records, we look to natural archives such as corals for geochemical paleoproxies. Corals offer exceptional chronological constraints and allow for approximately monthly-resolution climate and environmental proxy reconstruction over hundreds of years (Thompson, 2022 and references therein). It has long been known that skeleton cores from corals such as *Porites* spp., composed of the calcium carbonate polymorph aragonite, show luminescent layers under UV light (Isdale, 1984). The luminescence intensity of these bands correlates with freshwater run-off, as shown in multiple locations including

Australia (Rodriguez-Ramirez et al., 2014), Florida Bay (Smith et al., 1989) and Madagascar (Grove et al., 2013).

The luminescence is caused by the incorporation of humic-like substances into the coral skeleton during growth (Kaushal et al., 2020; Susic et al., 1991). Humic-like substances on land are formed from the breakdown of plant tissue, and after leaching into aquatic ecosystems they form an integral component of terrigenous CDOM and tDOC. Humic-like substances are rich in fluorescent aromatic moieties, and this fluorescence extends to longer wavelengths than that of coral skeletal aragonite. Therefore, when a coral core is illuminated with ultraviolet light, the ratios of emitted luminescence in the green wavelength band to that in the blue wavelength band (G/B ratio) measures downcore variability in the concentration of terrigenous humic-like substances, while normalizing for luminescence variation caused by changing coral skeletal structure (Grove et al., 2010; Kaushal et al., 2020). Moreover, we recently showed that luminescence G/B in a coral from Borneo tracks sub-annual terrigenous CDOM variability, as estimated from satellite-based measurements of the CDOM absorption coefficient at 440 nm (Kaushal et al., 2021). While luminescence G/B thus clearly has high potential as a paleoproxy for tDOM, reconstructing just CDOM absorption at a single wavelength can only give limited insights into land–ocean carbon flux dynamics. Here, we analyse two replicate coral cores collected from Singapore, where we collected ~monthly measurements over 2 years of CDOM absorption spectra, DOC concentration, and estimated tDOC concentration based on carbon stable isotopes (Zhou et al., 2021). We show that coral luminescence G/B can be used as a quantitative proxy to estimate tDOC concentration as well as the full CDOM absorption spectrum, demonstrating that this proxy can provide considerable insights into coastal carbon cycling in the tropics.

2. Material and methods

2.1 Study site and coral core collection

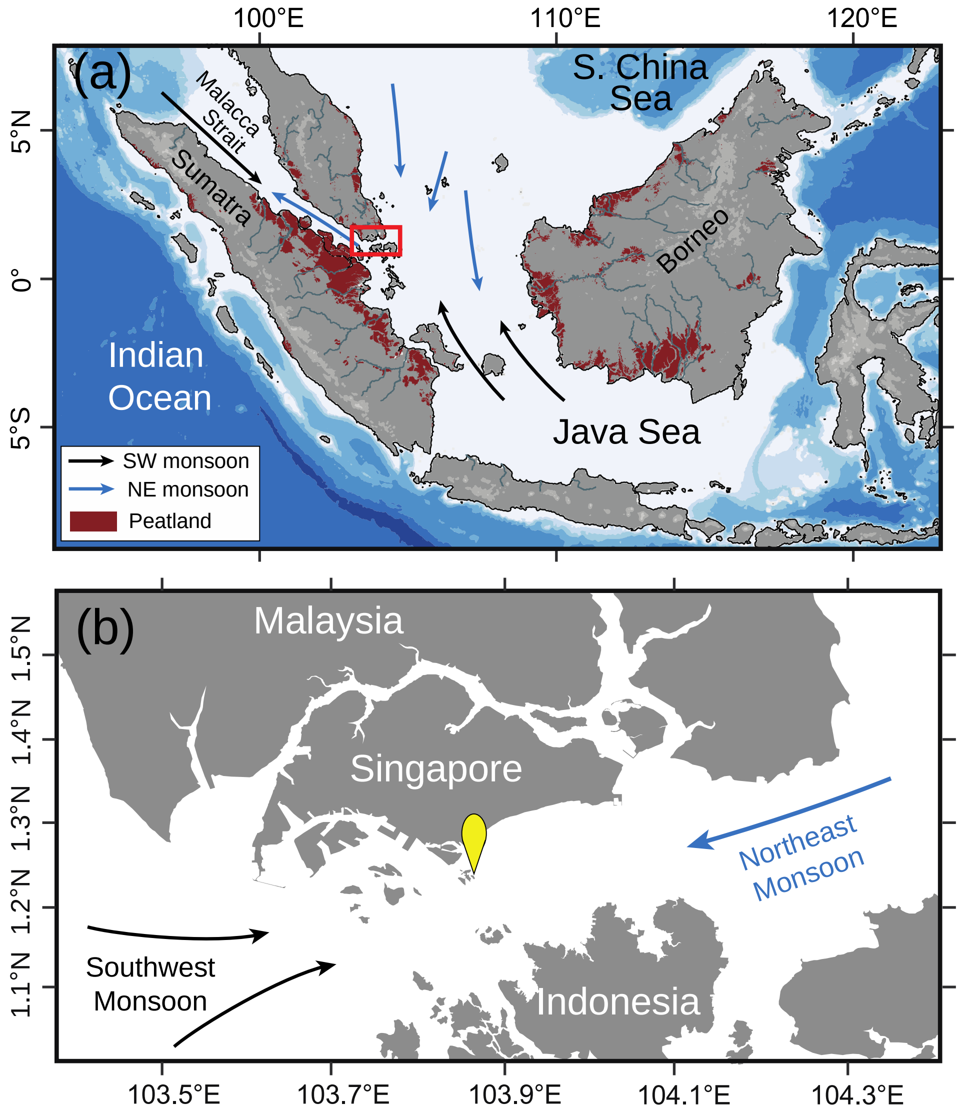

Figure 1: (a) Map of our study region showing the location of tropical peatlands and seasonal monsoon wind directions. During the northeast (NE) monsoon months, the currents transport waters from the South China Sea to our study region. During the southwest (SW) monsoon months, the currents reverse, transporting waters with inputs from tropical peatlands located on the east coast of Sumatra to our study site. Red rectangle indicates the region shown in panel (b). (b) Site for time series sampling and coral core collection in the Singapore Strait (yellow marker).

The Singapore Strait is located in the central Sunda Shelf Sea (Fig. 1) where water depths are mostly <50 m, and strong tidal currents fully mix the water column (Mayer and Pohlmann, 2014). The annual net circulation runs from the South China Sea into the Indian Ocean via the Malacca Strait owing to the pressure gradient between the South China Sea and the Andaman Sea that results from the basin-wide response to the monsoon winds. The monsoon system also causes seasonal reversal of currents, and during the peak southwest (SW) monsoon months from June to August, the current flows eastward from the coast of Sumatra through the Singapore Strait (van Maren and Gerritsen, 2012). Sumatra harbours the largest deposits of peat in Southeast Asia (Page et al., 2011) and the rivers draining these peatlands (which carry up to 5000 µmol l^{-1} DOC) are one of the most significant sources of tDOC to Southeast Asian coastal waters (Alkhatib et al., 2007; Baum et al., 2007; Rixen et al., 2008; Wit et al., 2018). The seasonally reversing currents thus result in seasonally high concentrations of tDOC and terrigenous CDOM in the Singapore Strait (Martin et al., 2021; Zhou et al., 2021).

One plug core was collected from the main growth axis of each two massive *Porites* spp. corals (KU-K and KU-L) off Kusu Island in the Singapore Strait (1.226°N 103.860°E, Fig. 1) at 2-3 m depth in Nov-2020, using an underwater electric drill with a 3 cm diameter, 30 cm length diamond bit core barrel. The cores were cleaned with water and sliced (~0.7 cm thick) using a rotary saw, and then further cleaned for 48 hours in a 1:4 dilution of household bleach (NaOCl, 3–7% reactive chlorine) and sonicated in deionized water for a total of 30 min (water changed every 10 min); this removes contaminants and increases the luminescence intensity (Nagtegaal et al., 2012). The KU-K core (hereafter KU-K) measures ~13 cm in length and has 11 visible couplets of dark and light bands. The KU-L plug core (hereafter KU-L) measures ~7 cm in length and has 7 visible couplets of dark and light bands (Figure 3). The seasonal timing of luminescent band formation in Singapore was previously ascertained through alizarin staining and repeated subsampling of tagged colonies (Tanzil et al., 2016). The dark bands in true colour images (bright bands in luminescence images) represent coral skeletal growth during the southwest monsoon period of high tDOC influx (Tanzil et al., 2016; Zhou et al., 2021). Here, we subsampled 4.8 cm of the KU-K and 3.0 cm of the KU-L cores, covering the growth period from the end of the SW monsoon in 2017 to core collection in Nov-2020.

2.2 Kusu seawater biogeochemical sampling

Biogeochemical sampling was conducted at Kusu once or twice per month at 5 m depth from Oct-2017 to Nov-2020. Details of collection, preservation, measurements and analysis of water samples are described in detail in Zhou et al., 2021 (Zhou et al., 2021), and are only briefly mentioned here and below (Section 2.3.1). Profiles of salinity and temperature were measured using a FastCTD Profiler (Valeport Ltd). Water samples for CDOM, DOC and $\delta^{13}C_{DOC}$ measurements were collected using a Niskin bottle and immediately filtered on the boat through a pre-rinsed 47 mm diameter, 0.22 µm pore-size polyethersulfone membrane filter (Supor, Merck Millipore) in an in-line filter housing connected to a peristaltic pump.

2.3 Experimental methods

2.3.1 Water sample analysis

CDOM absorption spectra were measured on a Thermo Evolution 300 dual-beam spectrophotometer in a 10-cm quartz cuvette from 230 to 900 nm. Ultrapure deionized water (18.2 MΩ cm^{-1}) was used as the reference. The CDOM absorbance (A_λ) was converted to absorption coefficient (a_λ) using:

$$a_\lambda = 2.303 \times (A_\lambda \div l) \quad (1)$$

where, a_λ and A_λ are, respectively, the absorption coefficient and the absorbance at wavelength λ, and *l* is the cuvette length in m. We refer to CDOM absorption at wavelength λ as $a_{CDOM}(\lambda)$. $SUVA_{254}$ is the specific UV absorbance at 254 nm and was calculated from the absorbance at 254 nm and the DOC concentration (Weishaar et al., 2003). The CDOM spectral slope $S_{275-295}$ and spectral slope ratio S_R (the ratio of $S_{275-295}$ to the spectral slope between 350-400 nm) were calculated as in Helms et al. (2008) (Helms et al., 2008). DOC samples (30 ml) were acidified with 100 µl 50% v/v H_2SO_4 and analyzed on a Shimadzu TOC-L system. Potassium hydrogen phthalate was used for calibration and accuracy was monitored using deep-sea certified reference material from the University of Miami, USA with a long-term reproducibility of 48.0 ± 3.9 µmol L^{-1}. The $\delta^{13}C_{DOC}$ samples were measured at the Jan Veizer Stable Isotope Laboratory, University of Ottawa Canada using an OI Analytical Aurora Model 1030W TOC Analyzer interfaced to a Finnigan Mat DeltaPlusXP isotope ratio mass spectrometer with a long-term reproducibility of ± 0.4 ‰. The spectral slope ratios were published in Martin et al., 2021 (Martin et al., 2021), while the remaining parameters (water temperature, salinity, CDOM absorption, $S_{275-295}$, $SUVA_{254}$, DOC concentration, $\delta^{13}C_{DOC}$) were published in Zhou et al, 2021 (Zhou et al., 2021). Here, we used monthly averaged values of the water measurements for comparison against coral data. We used the higher-resolution $a_{CDOM}(350)$ data *only* for age-depth model development.

2.3.2 Coral core luminescence, $\delta^{18}O$ and Sr/Ca measurements

Luminescence was measured parallel to the sampling track for Sr/Ca and $\delta^{18}O$ measurements. The cleaned KU-K and KU-L sections were scanned under ultraviolet light (365 nm) using spectral line scanning on an Avaatech XRF core scanner at the Asian School of the Environment following Grove et al. (2010) and Tanzil et al. (2016). The line scan camera records luminescence emission with the light source and recording camera progressing down the coral section as a single unit scanning multiple lines that are stitched together to produce a continuous core section image. The incoming light from the sample is split into three wavelength bands (red, green and blue) by a dichroic RGB beam splitter prism and recorded by separate sensors. Luminescence green-to-blue (G/B) measurements (or coral G/B) were obtained along the main growth axis for a 2 mm wide track at a resolution of 143 pixels cm^{-1} (~0.07 mm), with wavelength bands of green: 525-575 nm and blue: 425-475 nm. Ratioing to the blue band normalizes for changes to the luminescence signal resulting from downcore changes in coral density and architecture (Grove et al., 2010). Coral samples for Sr/Ca and $\delta^{18}O$ were drilled continuously at 1 mm resolution for Sr/Ca and $\delta^{18}O$ measurements. Further details of these measurements have been provided in Supplementary Information.

2.4 Theory and calculation

2.4.1 Estimating terrigenous Dissolved Organic Carbon (tDOC) concentration

Zhou et al. (2021) used a two-endmember mixing model to estimate the concentration of tDOC from our measured time series of DOC concentration and $\delta^{13}C_{DOC}$ in the Singapore Strait, and the estimated endmember $\delta^{13}C_{DOC}$ values for peatland-derived DOC (i.e., pure tDOC) and for marine DOC. The $\delta^{13}C_{DOC}$ endmember values (mean ± 1σ uncertainty) were taken as −29 ± 1‰ for peatland DOC, based on data from Sumatra, Borneo, and peninsular Malaysia, and as −21.88 ± 0.79‰ for autochthonous marine DOC, based on the Singapore Strait data during the late NE monsoon and inter-monsoon (late February-March, when the

Singapore Strait receives waters from the open South China Sea). The tDOC concentration for each sampling date was calculated by Zhou et al. (2021) as follows:

In our coastal sites, the measured DOC concentration (*$[DOC]_{meas}$*) is the sum of the terrigenous fraction (*[tDOC]*) and the marine fraction (*[mDOC]*):

$$[DOC]_{meas} = [tDOC] + [mDOC] \quad (2)$$

Also, the measured concentration of $DO^{13}C$ (*$[DO^{13}C]_{meas}$*) is the sum of the terrigenous fraction (*$[DO^{13}C]_{tDOC}$*) and the marine fraction (*$[DO^{13}C]_{mDOC}$*):

$$[DO^{13}C]_{meas} = [DO^{13}C]_{tDOC} + [DO^{13}C]_{mDOC} \quad (3)$$

The $[DO^{13}C]_{meas}$ is calculated from the measured DOC and $\delta^{13}C_{DOC}$ as:

$$[DO^{13}C]_{meas} \approx [DOC]_{meas} \times R_{meas} \quad (4)$$

where R_{meas} is the measured carbon isotope ratio, calculated as:

$$R_{meas} = (\delta^{13}C_{DOCmeas}(‰) \div 1000 + 1) \times R_{VPDB} \quad (5)$$

The $[DO^{13}C]_{tDOC}$ is approximated as:

$$[DO^{13}C]_{tDOC} \approx [tDOC] \times R_{tDOC} \quad (6)$$

where R_{tDOC} is the carbon isotope ratio of tDOC, and calculated using the riverine endmember of carbon isotopic composition of DOC:

$$R_{tDOC} = (\delta^{13}C_{DOCriver}(‰) \div 1000 + 1) \times R_{VPDB} \quad (7)$$

Similarly, R_{mDOC} is the carbon isotope ratio of marine DOC and is calculated in the same fashion from the marine DOC (mDOC) $\delta^{13}C$ endmember value. Equation 2 can then be rewritten as:

$$[DOC]_{meas} \times R_{meas} = [tDOC] \times R_{tDOC} + [mDOC] \times R_{mDOC} \quad (8)$$

where R_{mDOC} is the carbon isotope ratio of marine DOC, calculated using the marine endmember of carbon isotopic composition of DOC.

Solving Eqn. 2 and Eqn. 8 will return the concentration of terrigenous DOC.

2.4.2 Coral age-depth model

The age-depth models were created using coral G/B and our measured $a_{CDOM}(350)$, which has a pronounced SW monsoon peak (Zhou et al., 2021). Seasonal coral luminescence G/B at this site are distinct and cyclically reproducible between colonies from the same location, while skeletal density variations show a lack of discernable annual patterns (Tanzil et al., 2016). Sixty-three $a_{CDOM}(350)$ measurements were made at Kusu from Oct-2017 to Oct-2020, which provides a less ambiguous seasonal marker than water temperature or salinity (Supp. Fig. 1). QAnalySeries software was used to peak-align the 2018 and 2019 SW monsoon peaks in $a_{CDOM}(350)$ with corresponding peaks in coral G/B, providing an age-depth model for each core, yielding a growth rate of 16 mm $year^{-1}$ for KU-K and 10 mm $year^{-1}$ for KU-L. To further validate our age-depth model, we compared our temperature and salinity time series data to the coral Sr/Ca and $\delta^{18}O$ measurements.

2.4.3 Reconstructing full CDOM absorption spectra from coral G/B

We used two different methods to test whether coral G/B can be used to reconstruct full CDOM absorption spectra. In Method 1, we used coral G/B to reconstruct CDOM absorption at 300 nm and 400 nm, set the absorption at 700 nm to 0 m^{-1} (Green and Blough, 1994) and fit a first-order exponential curve through the three points. We also test a second approach (Method 2), in which we used coral G/B to reconstruct absorption at wavelength 350 and took the average the *measured* water CDOM spectral slope over the range 300–550 nm, and calculated the rest of the absorption spectrum following (Twardowski et al., 2004):

$$a_{\lambda} = a_{\lambda ref}\, e^{-S(\lambda - \lambda ref)} \qquad (9)$$

where a_λ and $a_{\lambda ref}$ are the absorption coefficients (m^{-1}) at wavelengths λ and λref, λref is the reference wavelength (350 nm in our case), and S is the spectral slope between 300–550 nm.

3. Results

3.1 Monsoon-driven seasonality of tDOC in the Singapore Strait

As previously described (Martin et al., 2021; Zhou et al., 2021), the Singapore Strait experiences a large input of tDOC and terrigenous CDOM during the SW monsoon (mid-May to mid-September, Fig. 3), when currents transport peatland-influenced waters from the east coast of Sumatra through the Singapore Strait. Consequently, there is a drop in salinity from ~33 to ~30, spikes in DOC concentration (>80 µmol kg^{-1}) and in CDOM absorption (a_{CDOM}(350) >0.5 m^{-1}) and $SUVA_{254}$ (>1.5 L mg^{-1} m^{-1}), large decreases in CDOM spectral slope $S_{275-295}$ (< 0.020 nm^{-1}) and in $\delta^{13}C_{DOC}$ (<-24 ‰), and high estimated tDOC concentrations (> 20 µmol kg^{-1}).

The early NE monsoon (December-January), when currents begin to transport open South China Sea water to the Singapore Strait, is also the season with most rainfall in Singapore and southern Malaysia. At this time, there is a smaller drop in salinity from 33 to 31, and lowest annual water temperatures of 28°C. DOC concentration increases to ~80 µmol kg^{-1}, comparable to the SW monsoon, but indicators of tDOM input show much smaller changes than during the SW monsoon: a_{CDOM}(350) is <0.5 m^{-1}, $SUVA_{254}$ ~1 L mg^{-1} m^{-1}, $\delta^{13}C_{DOC}$ ~-22.5‰, and $S_{275-295}$ ~0.025 nm^{-1}. The estimated tDOC concentration is therefore consistently <20 µmol kg^{-1}.

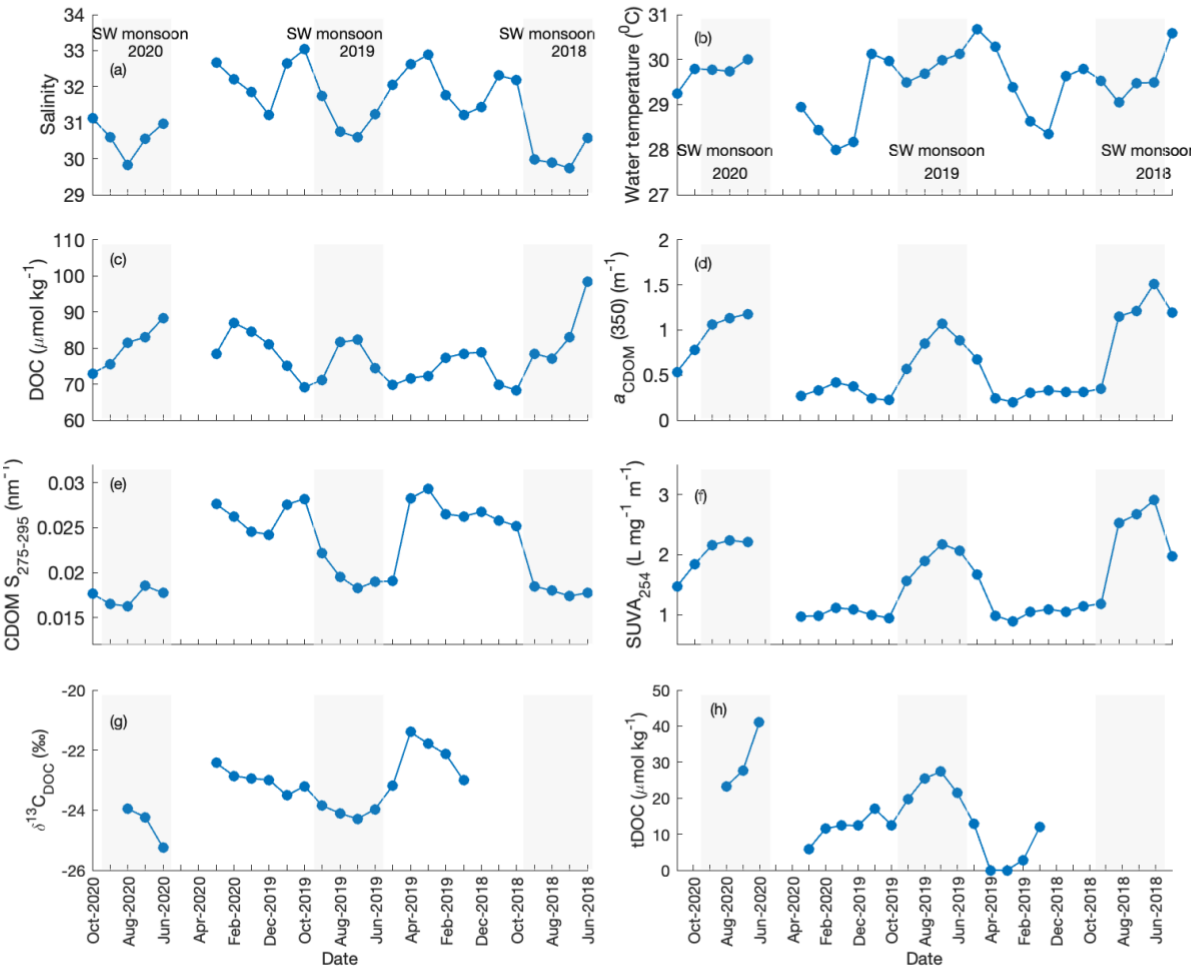

Figure 2: Monthly average biogeochemical data at Kusu Island (for full time series with all individual data, see (Martin et al., 2021; Zhou et al., 2021)). Note: The X-axis goes from younger-to-older from left-to-right to facilitate comparison with the coral data. (a) Salinity indicates a large input of freshwater during the SW monsoon (grey shading), while (b) water temperature shows limited seasonal variation with lowest temperature during the NE monsoon. (c) The bulk DOC pool shows clear peaks during the SW and NE monsoon, but (d-f) the CDOM parameters and (g) $\delta^{13}C_{DOC}$ show that a large input of tDOM only takes place during the SW monsoon. (h) Concentration of tDOC as calculated from the DOC concentration and the $\delta^{13}C_{DOC}$ data. The tDOC for March 2019 and April 2019 are less than zero, which is a result of using a single, fixed marine endmember value for $\delta^{13}C_{DOC}$ (from late February-March).

3.2 Coral age-depth model

Following the results from peak-aligning we use the KU-K section that grew from Jan-2018 to Feb-2020, and the KU-L section that grew from Oct-2017 to Nov-2019 for analysis in this study. These sections cover both the 2018 and 2019 SW monsoons, represented by bright layers in the coral luminescence images (Fig. 3a and 3b), dark brown colored bands in the true-colour images (Fig. 3c and 3d) and peaks in coral G/B ratio (Fig. 3e and 3f). The $a_{CDOM}(350)$ peak-aligned coral G/B values are shown in Fig. 3g.

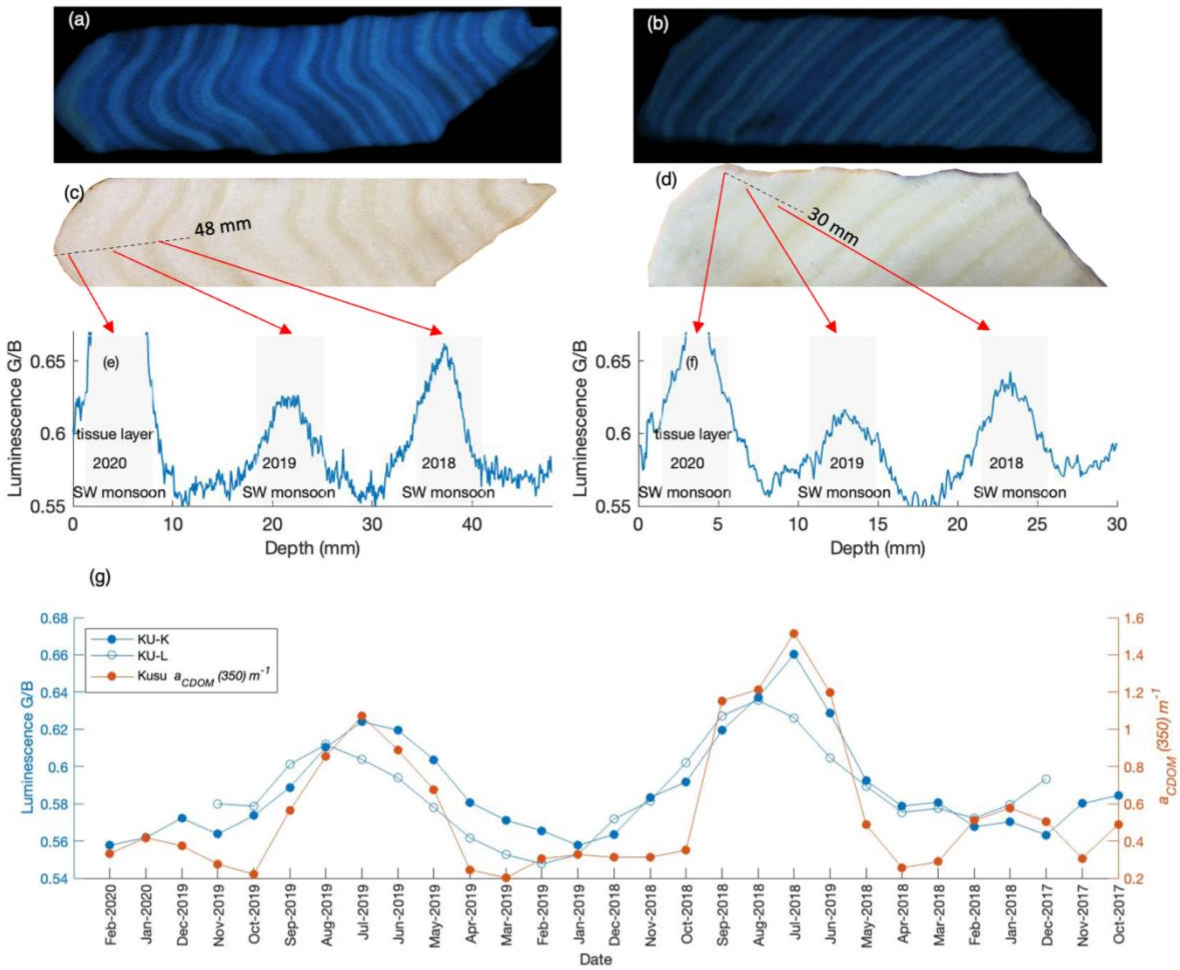

Figure 3: Coral luminescence G/B measurements. Luminescence (under ultraviolet excitation) and true-color images of coral plug cores (a,c) KU-K and (b,d) KU-L from Kusu Island. Dashed black lines in (c,d) indicate the growth axis along which luminescence G/B was quantified.

(e,f) The raw coral G/B measurements have been plotted against core depth. The core top 'tissue layers' show very high G/B and are omitted from our analysis. The approximate timing of the 2019 and 2018 SW monsoon periods are marked. (g) A monthly resolution age model was developed for the coral G/B by peak-aligning with measured $a_{CDOM}(350)$.

We then compared the measured temperature and salinity data to the corresponding coral Sr/Ca and $\delta^{18}O$ data according to our age-depth model (Supp. Fig. 2). In both cores, high water temperature coincides with low Sr/Ca, and high salinity coincides with high $\delta^{18}O$, which provides additional, independent validation of our age model.

3.3 Reconstructing tDOC and CDOM using coral G/B as a proxy

To test whether coral G/B ratios can track tDOC in coastal waters we compared coral G/B ratios with bulk DOC (which includes both the marine and terrigenous components of DOC; Fig. 4a), with $\delta^{13}C_{DOC}$ (where more negative values indicate a greater contribution from terrigenous DOC to the bulk DOC pool; Fig. 4b), and with our calculated tDOC concentration (Fig. 4c and 4d). The coral G/B ratio varied between 0.58 to 0.68 with distinct peaks in the SW monsoon, which coincided with the SW monsoon peak in bulk DOC (Fig. 4a). However, the coral G/B did not reflect the NE monsoon peak in bulk DOC, and coral G/B was therefore only poorly correlated with bulk DOC (KU-K R=0.21; KU-L R = 0.3; Fig. 4a). Coral G/B instead correlated well with $\delta^{13}C_{DOC}$ (KU-K R = -0.60; KU-L R = -0.86; Fig. 4b) and with calculated tDOC concentration (KU-K R = 0.64; KU-L R = 0.90; Fig. 4c,d). We then used the two regression models from Fig. 4c to reconstruct tDOC from the coral G/B records; this reconstruction has an RMSE of ±6.3 μmol kg^{-1}. Our reconstructed tDOC time series varies from 3 to 37 μmol kg^{-1} between Oct-2017 and Feb-2020, with both cores indicating higher tDOC concentrations during the 2018 SW monsoon than in 2019 (Fig. 4d).

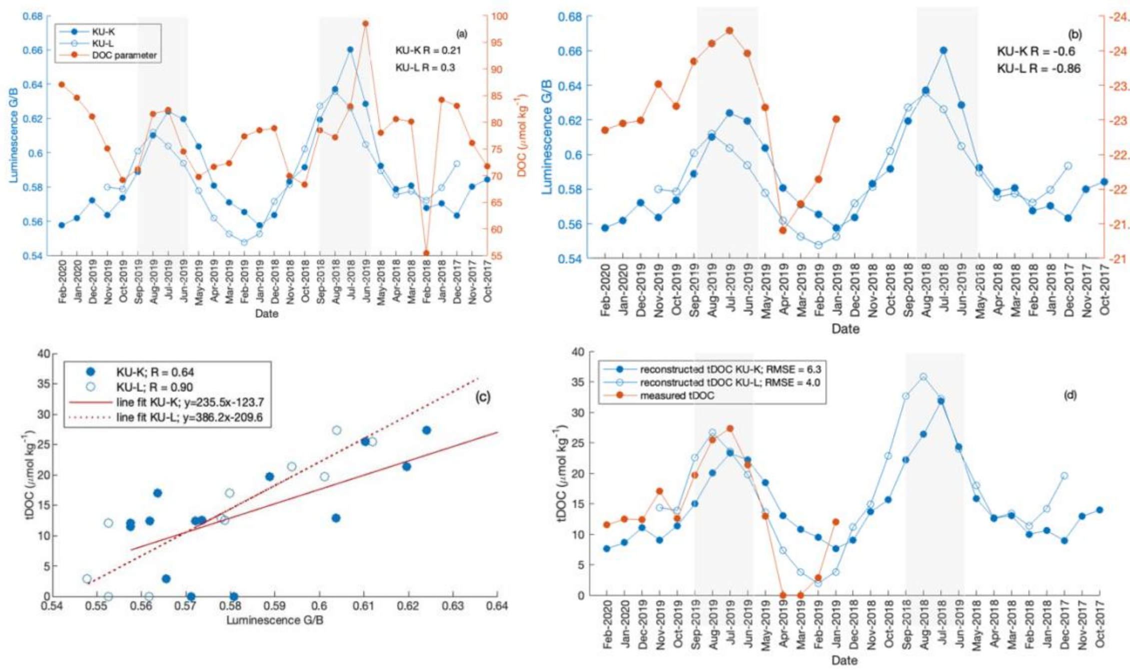

Figure 4: tDOC reconstruction using coral G/B measurements. (a) bulk DOC concentration, (b) $\delta^{13}C_{DOC}$, (c) coral G/B versus tDOC (d) and reconstructed tDOC have been plotted. tDOC has been calculated using the bulk DOC concentration and $\delta^{13}C_{DOC}$ measurements and an isotope mass balance approach. The relationship between measured coral G/B and tDOC has been used to reconstruct tDOC going back to Oct-2017. The measured tDOC and reconstructed tDOC values show RMSE values of 6.3 μmol kg^{-1} during the overlapping period from Jan-2019 to Feb-2020.

Moreover, coral G/B was strongly correlated (R >0.6) with monthly average CDOM absorption at every wavelength between 230 to 550 nm (Fig. 5a), which essentially covers the full wavelength spectrum of CDOM absorption. At wavelengths greater than 550 nm, monthly mean CDOM absorption was always <0.01 m^{-1} (Fig. 5b).

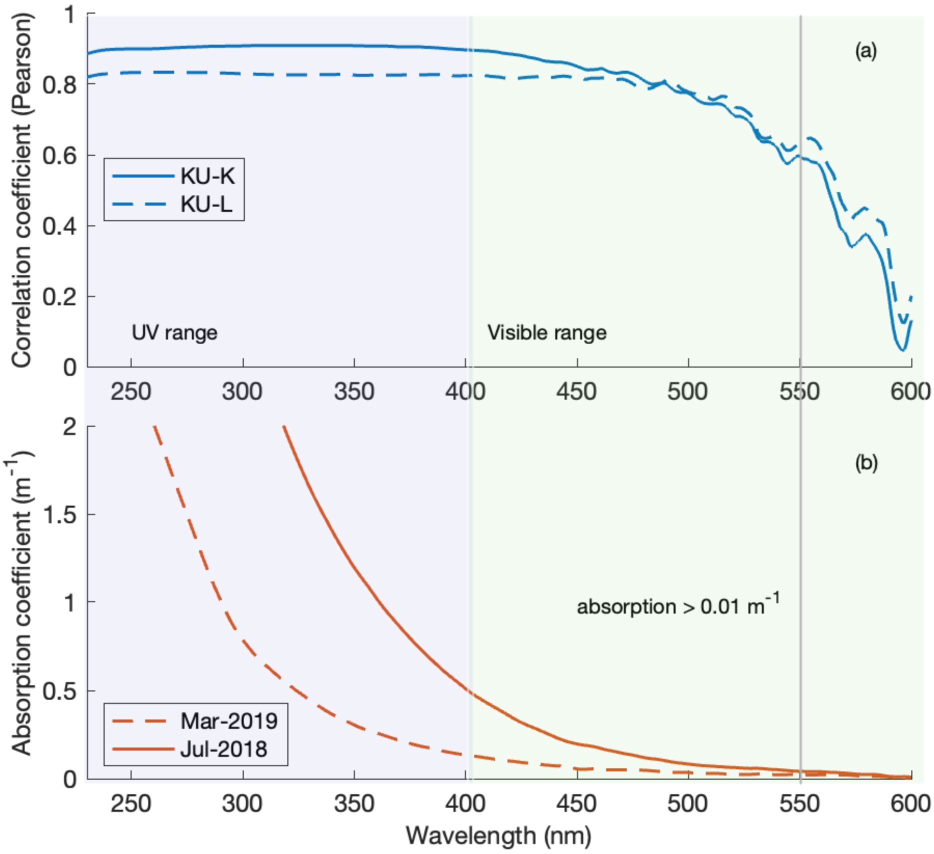

Figure 5: (a) Pearson's correlation coefficient between coral G/B and CDOM absorption coefficient at every wavelength between 230-600 nm. Strong correlations (R ≥0.6) are seen at all wavelengths up to 550 nm. (b) CDOM absorption spectra measured at Kusu in Mar-2019 and Jul-2018, which mark the lowest and highest CDOM absorption measured in our time series, respectively. At wavelengths greater than 550 nm, CDOM absorption was always <0.01 m^{-1}, which indicates that coral G/B correlates with CDOM absorption throughout the full CDOM absorption spectrum.

CDOM absorption and spectral slope parameters are a valuable way of comparing CDOM variability in different environments (Vantrepotte et al., 2015) in addition to providing independent information on the composition and biogeochemical processing of CDOM (e.g. (Helms et al., 2008; Weishaar et al., 2003). Of the CDOM parameters, coral G/B was most strongly correlated with $a_{CDOM}(350)$ (KU-K R = 0.91; KU-L R = 0.83; Fig 6a) and with

$SUVA_{254}$ (KU-K R = 0.89; KU-L R = 0.83; Fig. 6b), which are good tracers of terrigenous DOM in this region (Martin et al. 2018; 2021; Zhou et al. 2021). Coral G/B was also quite strongly correlated with the CDOM spectral slope parameters $S_{275\text{-}295}$ (KU-K R = -0.78; KU-L R = -0.76; Fig 6c) and slope ratio (KU-K R = -0.78; KU-L R = -0.73; Fig. 6d), although these correlations are weaker than for $a_{CDOM}(350)$ and $SUVA_{254}$ because $S_{275–295}$ and the slope ratio showed little difference between the 2018 and 2019 SW monsoons. $SUVA_{254}$ is emerging as a key measure to understand and model tDOC in the ocean (Anderson et al., 2019) and we found that coral G/B can also be used as a proxy to reconstruct $SUVA_{254}$, with low RMSE values of ±0.34 L mg^{-1} m^{-1} (Fig. 6e,f).

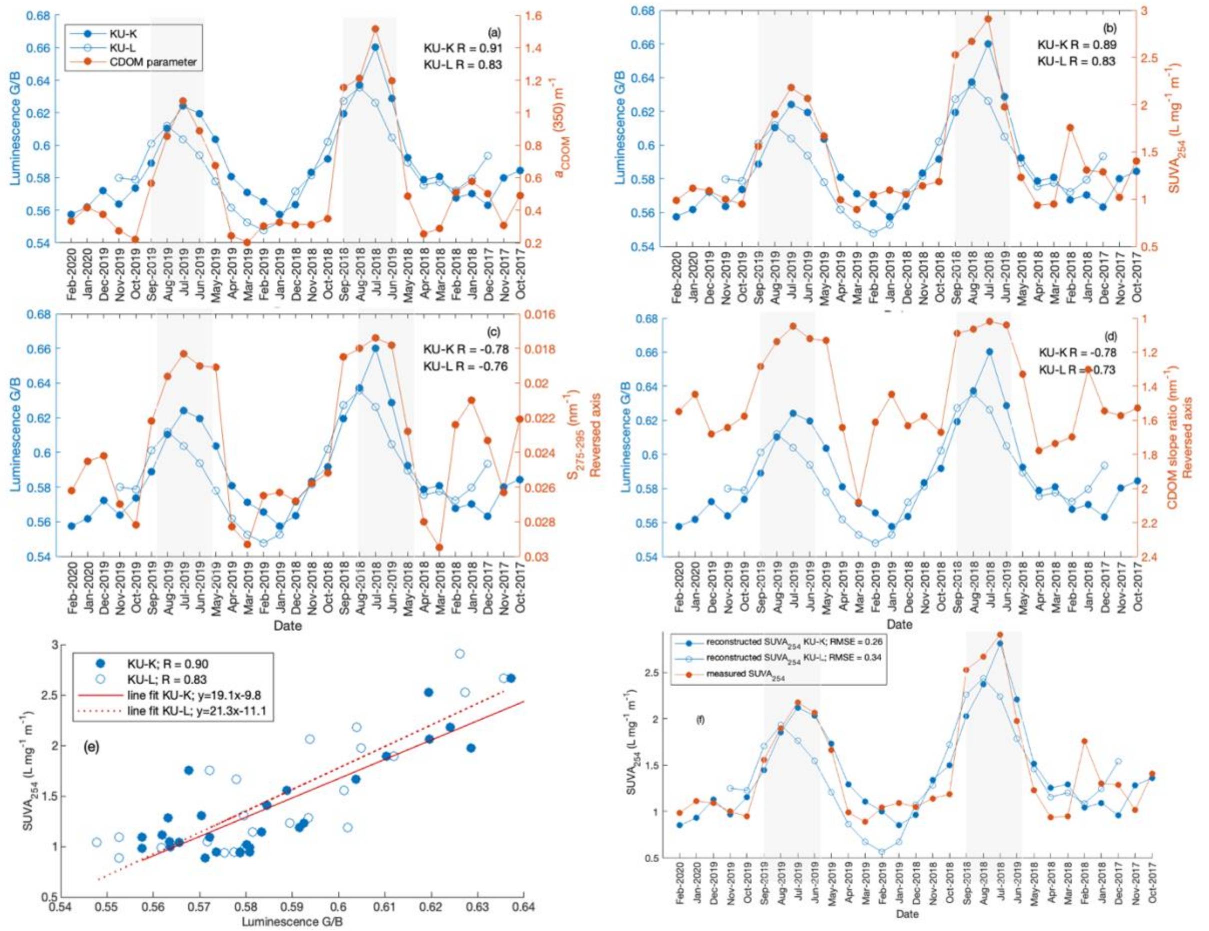

Figure 6: Coral G/B has been correlated (Pearson's correlation coefficient) with CDOM parameters relevant for tracing tDOM in the coastal ocean. The highest correlations are seen

with (a) $a_{CDOM}(350)$, and (b) $SUVA_{254}$, both of which trace terrigenous CDOM concentration in this region. The correlation is slightly lower for the spectral slope parameters (c) $S_{275-295}$ and (d) the slope ratio. Panels (e) and (f) demonstrate that coral G/B can be used to reconstruct $SUVA_{254}$ with low RMSE values of ±0.34 L mg^{-1} m^{-1}.

3.4 Reconstructing full CDOM spectra using coral G/B as a proxy

We tested two methods for reconstructing the full CDOM absorption spectrum: Method 1 simply reconstructs absorption at a limited number of points and estimates the full spectrum by fitting an exponential curve to the reconstructed points, while Method 2 requires an estimate of the CDOM spectral slope from field measurements. We find that both methods provide similarly accurate reconstructions of the CDOM absorption spectrum, as measured by the absolute and percentage RMSE between reconstructed and measured absorption at each wavelength, although Method 1 may perform very slightly better (Fig. 7). The linear models for reconstruction of absorption spectra, spectral slope measurements (from 300 to 550 nm) and plots of measured and reconstructed spectra are shown in supplementary figures 3, 4 and 5.

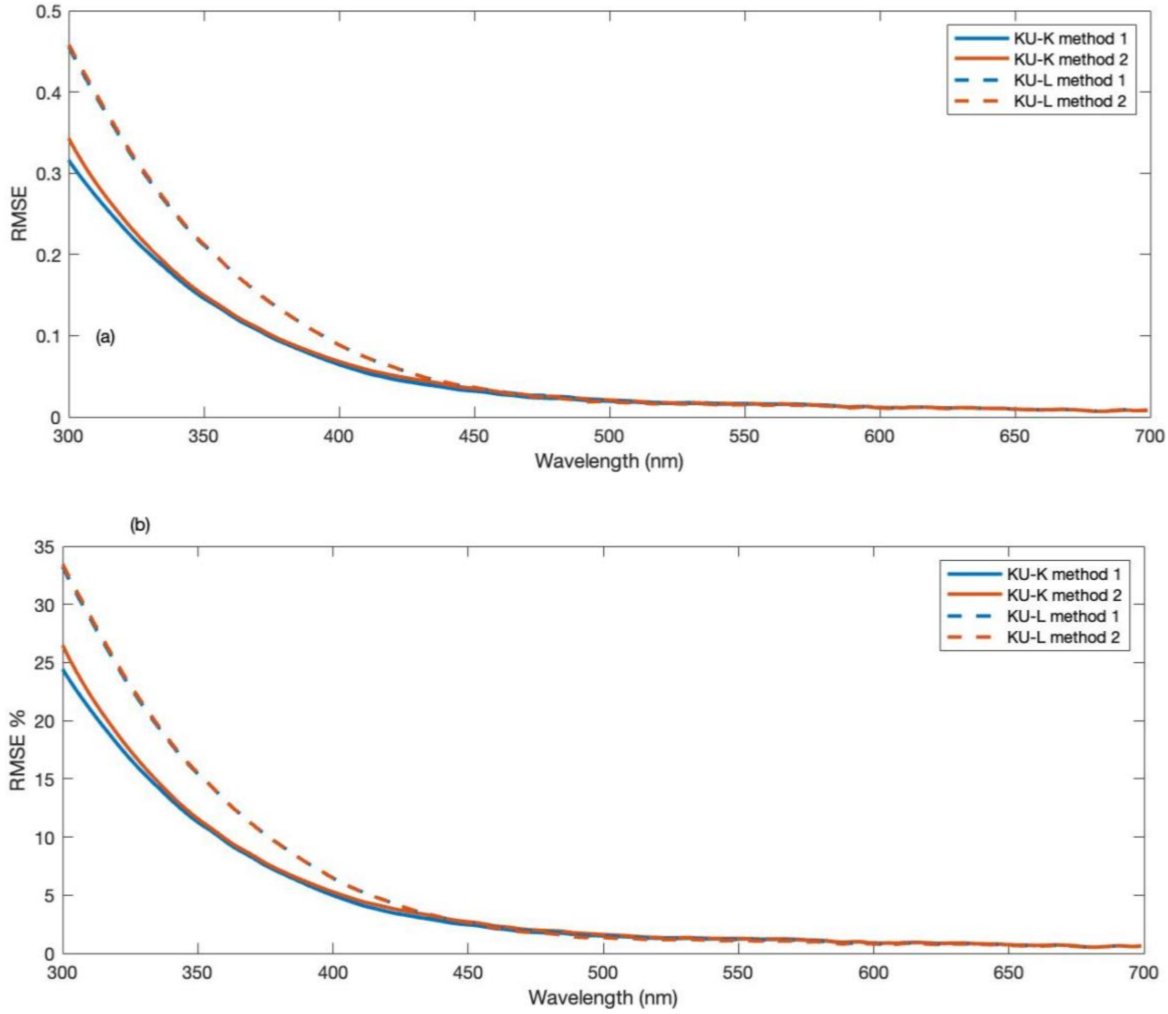

Figure 7: RMSE (300-700 nm) (a) and RMSE percentage (b) against wavelength between the measured CDOM spectra and spectra reconstructed from coral G/B using both reconstruction methods. Method 1 uses coral G/B to reconstruct absorption at wavelengths 300 and 400 nm, assumes 0 absorption at 700 nm, and fits a first-order exponential curve through these three points. Method 2 uses coral G/B to reconstruct absorption at wavelength 350 and uses the average CDOM spectral slope between 300-550 nm from in-situ CDOM measurements.

4. Discussion

4.1 tDOC source and seasonal variability

In this study, we use tDOC estimates calculated from carbon isotope mass balance calculations and CDOM parameters as measured by Zhou et al, 2021 to quantify tDOM at our study site. The terrigenous organic carbon in peatland-draining rivers into the Sunda Sea Shelf is overwhelmingly in the form of DOC (typically >95%) rather than POC (Alkhatib et al., 2007; Moore et al., 2011; Müller et al., 2015), so that our proposed proxy for tDOC captures the bulk of the terrigenous carbon input to the Sunda Shelf Sea. Coastal waters in the Sunda Shelf Sea receive relatively high tDOC inputs year-round (Sanwlani et al., 2022; Wit et al., 2018; Zhou et al., 2021). Although year-to-year variation in rainfall may cause some variation in the tDOC flux from peatlands, the seasonal variability in tDOC seen in Singapore is caused by the monsoonal reversals in ocean currents that bring peatland-influenced waters from the Sumatran coast in the SW monsoon, and open marine waters from the South China Sea during the NE monsoon (Zhou et al., 2021). The large and regular seasonal variation in tDOC at our site therefore make this a particularly suitable location for coral paleoproxy development.

4.2 Coral G/B is a sensitive proxy for tDOC concentration

Based on a simple linear relationship, we have found that tDOC can be reconstructed from coral G/B measurements with RMSE values of ±6.3 μmol kg^{-1}. The measured tDOC ranged from 0 to 30 μmol kg^{-1} with SW monsoon values of >20 μmol kg^{-1}. From our coral G/B-based reconstruction, we inferred a 10 μmol kg^{-1} difference in tDOC between the 2018 and 2019 SW monsoon peaks with a higher concentration in 2018 than 2019. This is also reflected in the measured CDOM parameters, bulk DOC concentration, and salinity, which suggested more freshwater input and higher concentration of tDOM in the Singapore Strait in 2018 compared to 2019 (Martin et al., 2021; Zhou et al., 2021).

Although the $\delta^{13}C_{DOC}$ suggests that there might be up to 10 µmol kg^{-1} tDOC during the NE monsoon period, the CDOM parameters such as $a_{CDOM}(350)$ and $SUVA_{254}$ show only small changes at this time (Fig. 6). This may indicate that the tDOC pool at this time is inherently less CDOM-rich and less aromatic, or that it has undergone more extensive prior biogeochemical processing that preferentially removed CDOM (e.g. photobleaching; see Helms et al., 2008; Martin et al., 2018). It is possible that less CDOM-rich and less aromatic-rich tDOM may be less well incorporated by corals. Abiotic precipitation experiments have shown that aragonite does not incorporate DOM indiscriminately, but preferentially incorporates peatland-derived DOM over marine DOM (Kaushal et al., 2020), which may be due to the variable structures of humic-like aromatic ring compounds and available sites for binding with calcium carbonate. However, coral cores also show luminescence due to terrestrial input in regions without peatlands (e.g. Grove et al., 2013), which shows that the G/B proxy is not just specific to peatland-derived tDOC.

Instead, it is possible that tDOC during the NE monsoon was overestimated, since it was calculated using a fixed value for the marine end-member $\delta^{13}C_{DOC}$, even though marine autochthonous carbon can span a relatively wide range of $\delta^{13}C$ values (Verwega et al., 2021). It is also not clear whether the peatland tDOC end-member $\delta^{13}C$ value used by (Zhou et al., 2021) is appropriate during the NE monsoon, because the most likely sources of tDOC during the NE monsoon would be local or regional input from the south and east coasts of the Malay Peninsula, where few peatlands are found (Fig. 1).

Overall, our data show that coral G/B can be a sensitive proxy for tDOC concentration, and that G/B is not affected by variation in the bulk concentration of marine autochthonous DOC. However, it is possible that coral G/B might not be less sensitive to some types of tDOC that are less aromatic and CDOM-rich, or that have undergone very extensive prior photobleaching. Knowledge of the regional tDOC sources their CDOM:DOC ratios, and of the possible extent of biogeochemical processing of the tDOC, is therefore advisable before applying this proxy in different regions.

4.3 Coral G/B can be used to reconstruct additional CDOM parameters that reflect DOM composition

CDOM parameters measure the absorption of light by DOM at different wavelengths, and DOM that originates from partial degradation of terrigenous vegetation is particularly light-absorbent (Massicotte et al., 2017; Vantrepotte et al., 2015a). This is reflected in the high CDOM absorption measured during the SW monsoon (Fig. 5). The high correlation of > 0.6 between the measured CDOM absorption and coral G/B ratio is consistent with the corals incorporating humic-like material of terrestrial origin. Of the different measured CDOM parameters, the coral G/B measurements showed highest correlation with $a_{\mathrm{CDOM}}(350)$ and with SUVA_{254} ($R > 0.83$). SUVA_{254} is strongly correlated with aromaticity (Weishaar et al., 2003), which fits well with our understanding of coral luminescence. SUVA_{254} was also recently proposed as a measure to distinguish tDOC pools according to their source and reactivity (especially as photolabile *versus* biolabile tDOC) in marine carbon cycle models (Anderson et al., 2019). However, SUVA_{254} data from tropical coastal oceans are scarce, so the fact that this parameter can be reconstructed with relatively good accuracy (RMSE of ±0.34 L mg^{-1} m^{-1}) from long coral cores may help to inform better marine carbon cycle models.

Compared to CDOM absorption coefficients and to $SUVA_{254}$, we found that coral G/B was slightly less strongly correlated with the CDOM spectral slope parameters $S_{275–295}$ and slope ratio. In particular, the spectral slope parameters did not reflect the difference between the 2018 and 2019 SW monsoons in tDOM input (as inferred from our in-situ CDOM, DOC, and salinity measurements). While both $S_{275–295}$ and slope ratio are very sensitive measures of the presence of tDOM (Fichot and Benner, 2011; Vantrepotte et al., 2015; Zhou et al., 2021), CDOM spectral slope properties change in a strongly non-linear manner when tDOM mixes with low-CDOM marine DOM, such that even small quantities of terrigenous CDOM initially lead to large changes in spectral slopes, but spectral slopes are then relatively insensitive to further increases in terrigenous CDOM (Stedmon and Markager, 2003). Hence, slope ratios might not be ideal measures of absolute concentration of tDOM and tDOC unless the terrigenous contribution is relatively low. The fact that coral G/B reflects variation in CDOM absorption coefficients and in $SUVA_{254}$ more closely than variation in CDOM spectral slope properties therefore suggests that coral G/B primarily traces the variation in absolute tDOM concentration.

The two methods of CDOM reconstruction from coral G/B work comparably well in our case. Method 1 fits an exponential curve through reconstructed points and has a slightly lower RMSE compared to Method 2 which uses spectral slope of CDOM from in-situ measurements. Method 2 requires in-situ measurements, which are also likely to have varied in the past, thus adding uncertainty to the paleo-reconstruction. Therefore, Method 1 provides a stronger approach for the reconstruction of CDOM.

4.4 Comparison to previous coral core calibration

In our previous work, we calibrated G/B ratios of a coral core collected off the coast of Borneo (Talang) with $a_{CDOM}(440)$ from satellite remote sensing, and also found a strong and linear relationship (Kaushal et al., 2021). Comparing the relationships for coral G/B to $a_{CDOM}(440)$ between our new, in-situ calibration from Kusu with the previous calibration from the Talang core (Fig. 8) reveals that the slopes of liner regressions are statistically indistinguishable since the standard errors (s.e.) of the slopes overlap (KU-K slope = 2.3 ± 0.3; KU-L slope = 2.6 ± 0.4; Talang slope = 2.1 ± 0.2). Moreover, a regression analysis of the combined dataset for all cores showed no significant interaction term between luminescence and coral core. However, there is a clear offset, with the Talang core having higher G/B for a given seawater $a_{CDOM}(440)$ value than either of the Kusu cores. This might simply reflect individual differences between coral colonies, although the fact that the two Kusu colonies have nearly identical calibrations might also indicate that there is a consistent difference in the tDOM pool between the sites. The Talang coral is located close to a peatland-draining river, and thus receives tDOM that is likely comparatively fresh and undegraded, given the predominantly conservative mixing pattern of tDOM in Talang coastal waters (Martin et al., 2018). In contrast, the Kusu cores receive tDOM from more distant rivers on Sumatra, and this tDOM has already undergone extensive remineralization and likely significant photobleaching in the coastal ocean prior to reaching the Singapore Strait (Zhou et al., 2021). Coral G/B is caused by the incorporation of a humic- and aromatic-rich fraction of the fluorescent tDOM pool, which itself is a subset of the light-absorbing CDOM pool. It is therefore possible that corals preferentially incorporate a relatively labile fraction of the tDOM pool (perhaps especially to photobleaching), in which case the observed offset between corals might be linked to how rich the terrigenous CDOM pool at each site is in this putatively labile tDOM fraction incorporated by the corals. Further research is clearly warranted to identify which chemical fractions of the tDOM pool contribute to coral G/B. Importantly, while our results suggest that local calibrations of coral G/B to measured tDOM parameters may be desirable, the similarity in calibration slopes between both sites suggests that at least relative variation in terrigenous CDOM can be inferred from coral G/B without a local calibration.

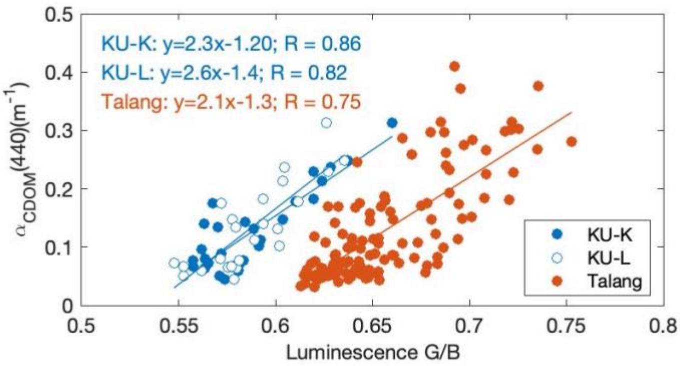

Figure 8: The relationship between coral G/B measurements of the KU-K and KU-L cores and measured $a_{CDOM}(440)$ is compared to the relationship between the Talang coral core G/B measurements and $a_{CDOM}(440)$ as estimated from satellite remote sensing (Kaushal et al., 2021). The offset on the luminescence axis may suggest that corals preferentially incorporate a relatively labile fraction of the tDOM pool; however, the similarity in slopes suggest that variability within a core nevertheless accurately reflects relative changes in CDOM absorption.

We find that we can reliably reconstruct full CDOM absorption spectra during high CDOM absorption periods (SW monsoon) at our study site. This provides information about changes in optical water quality that are important to fully understand the ecological effects of tDOM fluxes to coastal waters. In Singapore, the large seasonal variation in CDOM absorption leads to significant shoaling of the euphotic zone and causes a shift in underwater irradiance spectrum to longer wavelengths, which likely contributes to the seasonal change in phytoplankton pigment composition and to limiting the depth distribution of photosynthetic corals (Martin et al., 2021). Anthropogenic changes to tDOM input have been inferred to have similar impacts at several temperate sites as well (Aksnes et al., 2009). While coral G/B only provides information about variation in the terrigenous CDOM absorption spectrum, and thus cannot provide a complete description of the underwater light environment, the proxy may help to constrain relative variation in light penetration, especially in regions where information about particulate optical properties is available.

5. Conclusion

Our study demonstrates that monthly-resolution tDOC and CDOM variability in tropical coastal oceans can be reconstructed using coral cores. Given the long growth periods of coral cores extending back to several decades, our method provides a way to understand long-term drivers of tDOM to the coastal ocean. This is vital for better quantification of variability in land-to-ocean transfer of carbon, a significant component of the global carbon cycle, as well as to examine the ecological effects of coastal terrigenous CDOM variability.

Acknowledgements

Yongli Zhou, Chen Shuang, Molly Moynihan, Rob Nichols, Kyle Morgan, Kristy Chang, Woo Oon Yee and Chen Yuan assisted with fieldwork and laboratory analysis. We also thank the crew of Dolphin Explorer, Francis Yeo, Sapari and Surpato for enabling the fieldwork. This work was funded by the National Research Foundation, Singapore, Prime Minister’s Office, through an NRF–Royal Society Commonwealth Postdoctoral Fellowship to Nikita Kaushal (NRF-SCS-ICFC2017-01), through the Academic Research Fund Tier 1 grant from the Singapore Ministry of Education to Patrick Martin (Grant RG123/18), through the Marine Science Research and Development Programme grants MSRD-P32 to Patrick Martin and

MSRDP-P03 to Jani Tanzil and Nathalie F. Goodkin. The coral cores were collected under permit number NP/RP16-156-3b and seawater biogeochemical samples were collected under research permit NP/RP17-044-3 from the Singapore National Parks Board.

References

Aksnes, D.L., Dupont, N., Staby, A., Fiksen, Ø., Kaartvedt, S., Aure, J., 2009. Coastal water darkening and implications for mesopelagic regime shifts in Norwegian fjords. Mar. Ecol. Prog. Ser. 387, 39–49. https://doi.org/10.3354/meps08120

Alkhatib, M., Jennerjahn, T.C., Samiaji, J., 2007. Biogeochemistry of the Dumai River estuary, Sumatra, Indonesia, a tropical black-water river. Limnol. Oceanogr. 52, 2410–2417. https://doi.org/10.4319/lo.2007.52.6.2410

Anderson, T.R., Rowe, E.C., Polimene, L., Tipping, E., Evans, C.D., Barry, C.D.G., Hansell, D.A., Kaiser, K., Kitidis, V., Lapworth, D.J., Mayor, D.J., Monteith, D.T., Pickard, A.E., Sanders, R.J., Spears, B.M., Torres, R., Tye, A.M., Wade, A.J., Waska, H., 2019. Unified concepts for understanding and modelling turnover of dissolved organic matter from freshwaters to the ocean: the UniDOM model. Biogeochemistry 146, 105–123. https://doi.org/10.1007/s10533-019-00621-1

Baum, A., Rixen, T., Samiaji, J., 2007. Relevance of peat draining rivers in central Sumatra for the riverine input of dissolved organic carbon into the ocean. Estuar. Coast. Shelf Sci. 73, 563–570. https://doi.org/10.1016/j.ecss.2007.02.012

Butman, D.E., Wilson, H.F., Barnes, R.T., Xenopoulos, M.A., Raymond, P.A., 2015. Increased mobilization of aged carbon to rivers by human disturbance. Nat. Geosci. 8, 112–116. https://doi.org/10.1038/ngeo2322

Ciais, P., Sabine, C., Bala, G., Bopp, L., Brovkin, V., Canadell, J., Chhabra, A., DeFries, R., Galloway, J., Heimann, M., Jones, C., 2014. Carbon and other biogeochemical cycles. In Climate change 2013: the physical science basis. Contribution of Working Group I to the Fifth Assessment Report of the Intergovernmental Panel on Climate Change. Cambridge University Press, pp. 465–570.

Cole, J.J., Prairie, Y.T., Caraco, N.F., McDowell, W.H., Tranvik, L.J., Striegl, R.G., Duarte, C.M., Kortelainen, P., Downing, J.A., Middelburg, J.J., Melack, J., 2007. Plumbing the Global Carbon Cycle: Integrating Inland Waters into the Terrestrial Carbon Budget. Ecosystems 10, 172–185. https://doi.org/10.1007/s10021-006-9013-8

Dai, M., Yin, Z., Meng, F., Liu, Q., Cai, W.-J., 2012. Spatial distribution of riverine DOC inputs to the ocean: an updated global synthesis. Curr. Opin. Environ. Sustain., Carbon and nitrogen cycles 4, 170–178. https://doi.org/10.1016/j.cosust.2012.03.003

de Wit, H.A., Valinia, S., Weyhenmeyer, G.A., Futter, M.N., Kortelainen, P., Austnes, K., Hessen, D.O., Räike, A., Laudon, H., Vuorenmaa, J., 2016. Current Browning of Surface Waters Will Be Further Promoted by Wetter Climate. Environ. Sci. Technol. Lett. 3, 430–435. https://doi.org/10.1021/acs.estlett.6b00396

Drake, T.W., Van Oost, K., Barthel, M., Bauters, M., Hoyt, A.M., Podgorski, D.C., Six, J., Boeckx, P., Trumbore, S.E., Cizungu Ntaboba, L., Spencer, R.G.M., 2019. Mobilization of aged and biolabile soil carbon by tropical deforestation. Nat. Geosci. 12, 541–546. https://doi.org/10.1038/s41561-019-0384-9

Evans, C.D., Page, S.E., Jones, T., Moore, S., Gauci, V., Laiho, R., Hruška, J., Allott, T.E.H., Billett, M.F., Tipping, E., Freeman, C., Garnett, M.H., 2014. Contrasting vulnerability of drained tropical and high-latitude peatlands to fluvial loss of stored carbon. Glob. Biogeochem. Cycles 28, 1215–1234. https://doi.org/10.1002/2013GB004782

Fichot, C.G., Benner, R., 2011. A novel method to estimate DOC concentrations from CDOM absorption coefficients in coastal waters. Geophys. Res. Lett. 38. https://doi.org/10.1029/2010GL046152

Green, S.A., Blough, N.V., 1994. Optical absorption and fluorescence properties of chromophoric dissolved organic matter in natural waters. Limnol. Oceanogr. 39, 1903–1916. https://doi.org/10.4319/lo.1994.39.8.1903

Grove, C.A., Nagtegaal, R., Zinke, J., Scheufen, T., Koster, B., Kasper, S., McCulloch, M.T., van den Bergh, G., Brummer, G.J.A., 2010. River runoff reconstructions from novel spectral luminescence scanning of massive coral skeletons. Coral Reefs 29, 579–591. https://doi.org/10.1007/s00338-010-0629-y

Grove, C.A., Zinke, J., Peeters, F., Park, W., Scheufen, T., Kasper, S., Randriamanantsoa, B., McCulloch, M.T., Brummer, G.-J.A., 2013. Madagascar corals reveal a multidecadal signature of rainfall and river runoff since 1708. Clim. Past 9, 641–656. https://doi.org/10.5194/cp-9-641-2013

Helms, J.R., Stubbins, A., Ritchie, J.D., Minor, E.C., Kieber, D.J., Mopper, K., 2008. Absorption spectral slopes and slope ratios as indicators of molecular weight, source, and photobleaching of chromophoric dissolved organic matter. Limnol. Oceanogr. 53, 955–969. https://doi.org/10.4319/lo.2008.53.3.0955

Houghton, R.A., House, J.I., Pongratz, J., van der Werf, G.R., DeFries, R.S., Hansen, M.C., Le Quéré, C., Ramankutty, N., 2012. Carbon emissions from land use and land-cover change. Biogeosciences 9, 5125–5142. https://doi.org/10.5194/bg-9-5125-2012

Isdale, P., 1984. Fluorescent bands in massive corals record centuries of coastal rainfall. Nature 310, 578–579. https://doi.org/10.1038/310578a0

Kaushal, N., Sanwlani, N., Tanzil, J.T.I., Cherukuru, N., Sahar, S., Müller, M., Mujahid, A., Lee, J.N., Goodkin, N.F., Martin, P., 2021. Coral Skeletal Luminescence Records Changes in Terrestrial Chromophoric Dissolved Organic Matter in Tropical Coastal Waters. Geophys. Res. Lett. 48, e2020GL092130. https://doi.org/10.1029/2020GL092130

Kaushal, N., Yang, L., Tanzil, J.T.I., Lee, J.N., Goodkin, N.F., Martin, P., 2020. Sub-annual fluorescence measurements of coral skeleton: relationship between skeletal luminescence and terrestrial humic-like substances. Coral Reefs 39, 1257–1272. https://doi.org/10.1007/s00338-020-01959-x

Larsen, S., Andersen, T., Hessen, D.O., 2011. Climate change predicted to cause severe increase of organic carbon in lakes. Glob. Change Biol. 17, 1186–1192. https://doi.org/10.1111/j.1365-2486.2010.02257.x

Le Quéré, C., Andres, R.J., Boden, T., Conway, T., Houghton, R.A., House, J.I., Marland, G., Peters, G.P., van der Werf, G.R., Ahlström, A., Andrew, R.M., Bopp, L., Canadell, J.G., Ciais, P., Doney, S.C., Enright, C., Friedlingstein, P., Huntingford, C., Jain, A.K., Jourdain, C., Kato, E., Keeling, R.F., Klein Goldewijk, K., Levis, S., Levy, P., Lomas, M., Poulter, B., Raupach, M.R., Schwinger, J., Sitch, S., Stocker, B.D., Viovy, N., Zaehle, S., Zeng, N., 2013. The global carbon budget 1959–2011. Earth Syst. Sci. Data 5, 165–185. https://doi.org/10.5194/essd-5-165-2013

Martin, P., Cherukuru, N., Tan, A.S.Y., Sanwlani, N., Mujahid, A., Müller, M., 2018. Distribution and cycling of terrigenous dissolved organic carbon in peatland-draining rivers and coastal waters of Sarawak, Borneo. Biogeosciences 15, 6847–6865. https://doi.org/10.5194/bg-15-6847-2018

Martin, P., Sanwlani, N., Lee, T., Wong, J., Chang, K., Wong, E., Liew, S., 2021. Dissolved organic matter from tropical peatlands reduces shelf sea light availability in the Singapore Strait, Southeast Asia. Mar. Ecol. Prog. Ser. 672, 89–109. https://doi.org/10.3354/meps13776

Massicotte, P., Asmala, E., Stedmon, C., Markager, S., 2017. Global distribution of dissolved organic matter along the aquatic continuum: Across rivers, lakes and oceans. Sci. Total Environ. 609, 180–191. https://doi.org/10.1016/j.scitotenv.2017.07.076

Mayer, B., Pohlmann, T., 2014. Simulation of Organic Pollutants: First Step towards an Adaptation to the Malacca Strait. Asian J. Water Environ. Pollut. 11, 75–86.

Monteith, D.T., Stoddard, J.L., Evans, C.D., de Wit, H.A., Forsius, M., Høgåsen, T., Wilander, A., Skjelkvåle, B.L., Jeffries, D.S., Vuorenmaa, J., Keller, B., Kopácek, J., Vesely, J., 2007. Dissolved organic carbon trends resulting from changes in atmospheric deposition chemistry. Nature 450, 537–540. https://doi.org/10.1038/nature06316

Moore, S., Evans, C.D., Page, S.E., Garnett, M.H., Jones, T.G., Freeman, C., Hooijer, A., Wiltshire, A.J., Limin, S.H., Gauci, V., 2013. Deep instability of deforested tropical peatlands revealed by fluvial organic carbon fluxes. Nature 493, 660–663. https://doi.org/10.1038/nature11818

Moore, S., Gauci, V., Evans, C.D., Page, S.E., 2011. Fluvial organic carbon losses from a Bornean blackwater river. Biogeosciences 8, 901–909. https://doi.org/10.5194/bg-8-901-2011

Müller, D., Warneke, T., Rixen, T., Müller, M., Jamahari, S., Denis, N., Mujahid, A., Notholt, J., 2015. Lateral carbon fluxes and CO_2 outgassing from a tropical peat-draining river. Biogeosciences 12, 5967–5979. https://doi.org/10.5194/bg-12-5967-2015

Nagtegaal, R., Grove, C.A., Kasper, S., Zinke, J., Boer, W., Brummer, G.-J.A., 2012. Spectral luminescence and geochemistry of coral aragonite: Effects of whole-core treatment. Chem. Geol. 318–319, 6–15. https://doi.org/10.1016/j.chemgeo.2012.05.006

Noacco, V., Wagener, T., Worrall, F., Burt, T.P., Howden, N.J.K., 2017. Human impact on long-term organic carbon export to rivers. J. Geophys. Res. Biogeosciences 122, 947–965. https://doi.org/10.1002/2016JG003614

Page, S.E., Rieley, J.O., Banks, C.J., 2011. Global and regional importance of the tropical peatland carbon pool. Glob. Change Biol. 17, 798–818. https://doi.org/10.1111/j.1365-2486.2010.02279.x

Rixen, T., Baum, A., Pohlmann, T., Balzer, W., Samiaji, J., Jose, C., 2008. The Siak, a tropical black water river in central Sumatra on the verge of anoxia. Biogeochemistry 90, 129–140. https://doi.org/10.1007/s10533-008-9239-y

Rodriguez-Ramirez, A., Grove, C.A., Zinke, J., Pandolfi, J.M., Zhao, J., 2014. Coral Luminescence Identifies the Pacific Decadal Oscillation as a Primary Driver of River Runoff Variability Impacting the Southern Great Barrier Reef. PLOS ONE 9, e84305. https://doi.org/10.1371/journal.pone.0084305

Sanwlani, N., Evans, C.D., Müller, M., Cherukuru, N., Martin, P., n.d. Rising dissolved organic carbon concentrations in coastal waters of northwestern Borneo related to tropical peatland conversion. Sci. Adv. 8, eabi5688. https://doi.org/10.1126/sciadv.abi5688

Smith, I., Thomas J., Hudson, H.J., Robblee, M.B., Powell, G.N., Isdale, P.J., 1989. Freshwater Flow from the Everglades to Florida Bay: A Historical Reconstruction Based on Fluorescent Banding in The Coral Solenastrea Bournoni. Bull. Mar. Sci. 44, 274–282.

Stedmon, C.A., Markager, S., 2003. Behaviour of the optical properties of coloured dissolved organic matter under conservative mixing. Estuar. Coast. Shelf Sci. 57, 973–979. https://doi.org/10.1016/S0272-7714(03)00003-9

Susic, M., Boto, K., Isdale, P., 1991. Fluorescent humic acid bands in coral skeletons originate from terrestrial runoff. Mar. Chem. 33, 91–104. https://doi.org/10.1016/0304-4203(91)90059-6

Tanzil, J.T.I., Lee, J.N., Brown, B.E., Quax, R., Kaandorp, J.A., Lough, J.M., Todd, P.A., 2016. Luminescence and density banding patterns in massive Porites corals around the Thai-Malay Peninsula, Southeast Asia. Limnol. Oceanogr. 61, 2003–2026. https://doi.org/10.1002/lno.10350

Thompson, D.M., 2022. Environmental records from coral skeletons: A decade of novel insights and innovation. WIREs Clim. Change 13, e745. https://doi.org/10.1002/wcc.745

Twardowski, M.S., Boss, E., Sullivan, J.M., Donaghay, P.L., 2004. Modeling the spectral shape of absorption by chromophoric dissolved organic matter. Mar. Chem., CDOM in the Ocean: Characterization, Distribution and Transformation 89, 69–88. https://doi.org/10.1016/j.marchem.2004.02.008

Urtizberea, A., Dupont, N., Rosland, R., Aksnes, D.L., 2013. Sensitivity of euphotic zone properties to CDOM variations in marine ecosystem models. Ecol. Model. 256, 16–22. https://doi.org/10.1016/j.ecolmodel.2013.02.010

van Maren, D.S., Gerritsen, H., 2012. Residual flow and tidal asymmetry in the Singapore Strait, with implications for resuspension and residual transport of sediment. J. Geophys. Res. Oceans 117. https://doi.org/10.1029/2011JC007615

Vantrepotte, V., Danhiez, F.-P., Loisel, H., Ouillon, S., Mériaux, X., Cauvin, A., Dessailly, D., 2015. CDOM-DOC relationship in contrasted coastal waters: implication for DOC retrieval from ocean color remote sensing observation. Opt. Express 23, 33–54. https://doi.org/10.1364/OE.23.000033

Verwega, M.-T., Somes, C.J., Schartau, M., Tuerena, R.E., Lorrain, A., Oschlies, A., Slawig, T., 2021. Description of a global marine particulate organic carbon-13 isotope data set. Earth Syst. Sci. Data 13, 4861–4880. https://doi.org/10.5194/essd-13-4861-2021

Wauthy, M., Rautio, M., Christoffersen, K.S., Forsström, L., Laurion, I., Mariash, H.L., Peura, S., Vincent, W.F., 2018. Increasing dominance of terrigenous organic matter in circumpolar freshwaters due to permafrost thaw. Limnol. Oceanogr. Lett. 3, 186–198. https://doi.org/10.1002/lol2.10063

Weishaar, J.L., Aiken, G.R., Bergamaschi, B.A., Fram, M.S., Fujii, R., Mopper, K., 2003. Evaluation of Specific Ultraviolet Absorbance as an Indicator of the Chemical Composition and Reactivity of Dissolved Organic Carbon. Environ. Sci. Technol. 37, 4702–4708. https://doi.org/10.1021/es030360x

Wit, F., Rixen, T., Baum, A., Pranowo, W.S., Hutahaean, A.A., 2018. The Invisible Carbon Footprint as a hidden impact of peatland degradation inducing marine carbonate dissolution in Sumatra, Indonesia. Sci. Rep. 8, 17403. https://doi.org/10.1038/s41598-018-35769-7

Zhou, Y., Evans, C.D., Chen, Y., Chang, K.Y.W., Martin, P., 2021. Extensive Remineralization of Peatland-Derived Dissolved Organic Carbon and Ocean Acidification in the Sunda Shelf Sea, Southeast Asia. J. Geophys. Res. Oceans 126, e2021JC017292. https://doi.org/10.1029/2021JC017292